Subsurface Oxygen Stabilization by a Third Species: Carbonates on Ag(210)

Letizia Savio,*,† Andrea Gerbi,† Luca Vattuone,† Raghani Pushpa,‡ Nicola Bonini,‡ Stefano de Gironcoli,‡ and Mario Rocca§

CNISM−Unita' di Genova, IMEM-CNR, and Dipartimento di Fisica, Universitá di Genova, Via Dodecaneso 33, 16146 Genova, and SISSA and INFM DEMOCRITOS National Simulation Centre, via Beirut 2-4, 34014, Trieste, Italy

Received: February 20, 2007; In Final Form: May 17, 2007

Subsurface species have often been invoked to explain the activation of catalytic surfaces for specific reactions. In particular, subsurface oxygen is thought to be important for the chemistry of Ag catalysts. Here we show by experimental and theoretical methods that on Ag(210) subsurface oxygen is stabilized by carbonates more efficiently than by O adatoms, thus leading to a concentration up to 4 times larger in the presence of the former adsorbate. Experimentally, a maximum of six subsurface O atoms are found to be stabilized by each carbonate. These results might be relevant for the current efforts to bridge the structure and pressure gaps between surface science and industrial conditions, for which non-negligible amounts of carbonates are surely present.

Introduction

Subsurface species have often been suggested to be responsible for the activation of catalyst surfaces for particular reactions.[1] Ag is intriguing in this respect, since oxygen dissolves easily into the bulk and subsurface oxygen has been suggested to play a pivotal role in several catalytic reactions, e.g., in activating oxygen for ethylene epoxidation[2−4] and for partial oxidation of methanol to formaldehyde[5] and in increasing the reaction probability for selective CO oxidation in the presence of H_2.[6] In particular, Ag powders have a unique selectivity for the first reaction, which has not been reproduced so far under controlled ultra-high-vacuum conditions, in spite of extensive research. On the other hand, ethylene epoxide formation was observed in the 10^{-2} mbar pressure range after pretreatment of polycrystalline silver with an O_2 and CO mixture,[7,8] an effect suggested to be related to subsurface oxygen accumulation, as originally predicted by theory.[2] Although the active role of subsurface (O_{sub}) and/or of dissolved oxygen in ethylene epoxide production has recently been questioned,[9−11] the contrasting literature on this topic[7,12,13] demonstrates that the issue is still controversial.

For their very nature subsurface species are hard to monitor experimentally with the usual surface-sensitive spectroscopies. Recently, we showed that on Ag(210) super- and subsurface oxygen can be distinguished by X-ray photoemission spectroscopy (XPS)[14] and that they give rise to a dipole active vibration at 56 meV,[15] corresponding to the in-phase motion of O in super- and subsurface sites against the Ag lattice.[16]

Here we report on a combined high-resolution electron energy loss spectroscopy (HREELS), time-resolved XPS, and density functional theory (DFT) investigation of CO oxidation on Ag(210). We find oxygen adatoms to be extremely reactive toward CO oxidation. The produced CO_2 desorbs, but at a low crystal temperature ($T = 110$ K), its lifetime at the surface is long enough to allow for further oxidation to CO_3, which remains adsorbed. During this process some extra O accumulates in subsurface sites, implying that this species is stabilized by CO_3 even more efficiently than by O adatoms. From the experimental data we estimate that a maximum of six oxygens lie in the interstitials below each carbonate. Such a result is consistent with DFT calculations, which were however performed only for a maximum of three subsurface oxygens per CO_3 group. This finding represents a significant step onward in the current efforts to bridge the structure and pressure gaps between controlled surface science conditions and industrial reactors, in which a non-negligible amount of carbonates surely forms and hence carbonate-induced, subsurface oxygen accumulation is likely to occur. The mechanism presented here might thus be of relevance for all catalytic reactions favored by O_{sub} accumulation.

Experimental and Computational Details

XPS experiments were carried out at the SuperESCA beamline of the ELETTRA synchrotron radiation source in Trieste,[17] while HREELS measurements were performed in Genova.[18] Both experimental apparatuses were equipped with a supersonic molecular beam, which allows us to select the energy E_i of the impinging molecules. For the experiments we used a pure O_2 beam ($E_i = 0.10$ eV) or O_2 seeded in helium (3% concentration, $E_i = 0.40$ eV). The beam flux was $\phi = 0.03$ ML/s (ML = monolayer, 1 ML = 1.07×10^{15} atoms/cm^2) in Trieste and $\phi = 0.08$ ML/s in Genova for pure O_2 and 0.03 ML/s in Trieste and 0.04 ML/s in Genova for the seeded beam. CO was dosed by backfilling the chamber. XPS measurements were recorded while dosing, thus allowing for a time-resolved investigation on a 10 s time scale.[19] Oxygen was dosed with the beam impinging perpendicularly to the (210) plane; the photoelectron emission angle was $\theta_{em} = 40°$.

To maximize the surface sensitivity and the XPS cross section, the C1s and the O1s regions were investigated with

* To whom correspondence should be addressed. E-mail: savio@fisica.unige.it. Phone: +39 010 3536292. Fax: +39 010 3622790.

† CNISM−Unita' di Genova and Dipartimento di Fisica, Universitá di Genova.

‡ SISSA and INFM DEMOCRITOS National Simulation Centre.

§ IMEM-CNR and Dipartimento di Fisica, Universitá di Genova.

10.1021/jp0714421 CCC: $37.00
Published on Web 06/28/2007

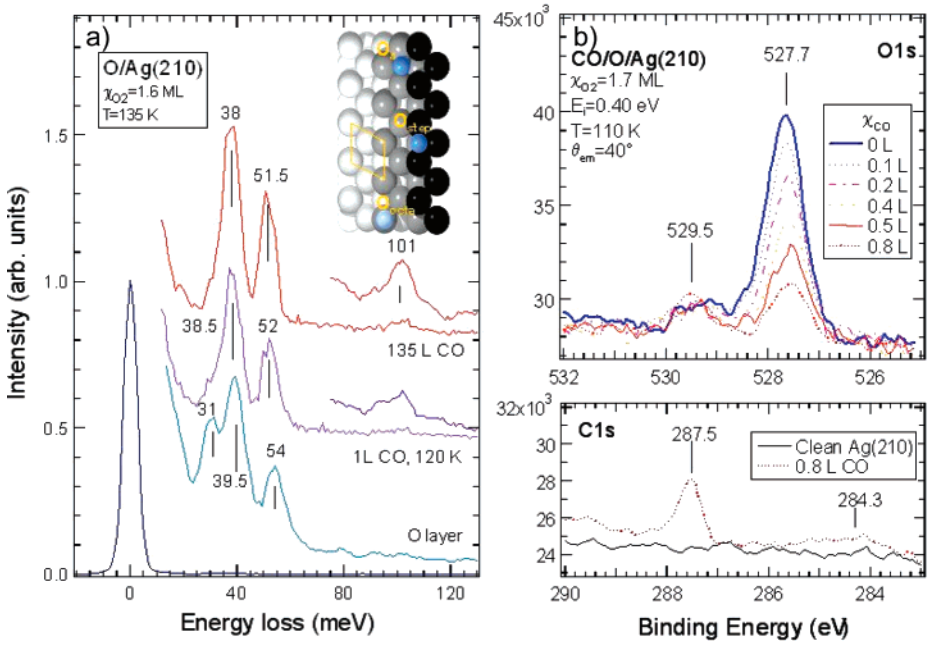

Figure 1. (A) HREEL spectra for CO oxidation on Ag(210). After 1 langmuir of CO exposure the 31 meV peak has been completely removed while the 39.5 and 54 meV peaks have downshifted to 38.5 and 52 meV, respectively. A much larger dose causes further minor downshifts and the appearance of the carbonate vibrational signature at 101 meV. (B) Corresponding experiment monitored by XPS. We note that most of the supersurface oxygen is removed already after 0.8 lanmuir of CO due to CO oxidation. The reaction causes CO_2 (desorbing) and CO_3 (287.5 eV peak) formation. Inset of panel a: Schematic drawing of the Ag(210) geometry (top view). The unit cell and the relevant sites for oxygen adsorption are indicated.

photon energies hν = 400 and 655 eV, respectively. The overall resolution was 0.15 and 0.30 eV in the two cases. The relative sensitivity to C and O was determined by comparing the signal intensities recorded for CO_2 adsorption under CO_2 pressure. We found that the sensitivity to C is ~7.5 times larger than that to O,[20] in fair agreement with the value estimated from the photoionization cross section of the two elements and from the photon flux at the two primary energies. The energy of the photoemitted electrons is calibrated with respect to the Fermi edge recorded at T = 93 K for each measuring condition. The $Ag3d_{5/2}$ level is then at 368.25 eV, in accord with the value reported in the literature.[21] Peak areas are estimated via a best fit procedure based on the Doniac−Sunjic function. The estimated error in the determination of the peak position is 50 meV. The relative error in the calculated areas is between 5% and 20%, depending on the quality of the original spectra.

HREEL spectra are recorded in-specular, with a primary electron energy E_e = 1.35 eV and a typical resolution of 6 meV. The Ag sample is a 7 mm diameter disk cut within 0.1° along the (210) plane. Its structure is schematically reported in the inset of Figure 1: it consists of alternating, one-atom-row-wide (100) and (110) nanofacets and is therefore characterized by a 50% density of open steps. Before each experiment the sample is prepared by sputtering cycles followed by annealing to 700 K until no contamination is detected by HREELS or XPS and a sharp LEED pattern is observed. Residual traces of carbon are removed by O_2 exposure at 600 K.

Density functional theory total energy and vibrational linear-response (density functional perturbation theory (DFPT)) calculations were performed using the PWscf and Phonon codes in the Quantum ESPRESSO[22] distribution. The pseudopotential formalism with ultrasoft pseudopotentials[23] and a plane-wave basis set up to a kinetic energy cutoff of 27 Ry (216 Ry for charge density) were used. Exchange and correlation effects were described at the generalized-gradient approximation (GGA) level employing the Perdew−Burke−Ernzerhof (PBE) functional.[24] Brillouin zone (BZ) integration has been performed with the Methfessel−Paxton smearing[25] technique using a smearing width of 0.03 Ry and a (3 × 5 × 1) Monkhorst−Pack mesh.[26] To model the surface, we used periodic supercells. The Ag(210) surface is modeled with a slab of 10 (210) layers; adjacent slabs were separated by a vacuum region of at least 16 au. Oxygen and CO_3 were adsorbed on both sides of the slab. In our calculations, we used supercells with (2 × 1) and (2 × 2) surface periodicity, resulting in CO_3 coverages of 0.5 and 0.25 ML, respectively. The (2 × 1) supercell contains 20 Ag atoms, and the (2 × 2) supercell contains 40 Ag atoms. The attained coverages are much larger than the experimentally observed ones, thus making difficult an exact comparison with experimental data. Performing calculations on much lower coverages would, however, require a significant increase of computational resources.

Results and Discussion

Spectra from the HREELS experiment are shown in Figure 1A. The oxygen layer was produced by exposing the Ag(210) surface at a crystal temperature T = 135 K to 1.6 MLs of O_2 with E_i = 0.40 eV. The oxygen adatom coverage, $\Theta_{O_{ad}}$, was ~0.16 ML as determined from O_2 uptakes performed under identical conditions and measured with the retarded reflector method.[14,15] Adsorption is dissociative, as witnessed by the three losses at 31, 39.5, and 54 meV. The first two modes are identified with O adatoms in 4-fold hollows (O_4) and at step edges (O_{step}), respectively.[15] The last one is connected to subsurface oxygen and arises from the in-phase vibration of O_{step} and O in subsurface octahedral sites (O_{octa}) against the Ag lattice.[16] Upon exposure to 1 langmuir of CO at 120 K, the 31 meV species disappears, the intermediate peak moves to 38.5 meV, and the highest energy loss downshifts to 52 meV. CO dosing increases the electron reflectivity approximately by a factor of 5, in accord with the surface cleansing action produced by oxidation. After 135 langmuirs of CO, a loss appears at 101 meV, indicating carbonate formation,[27] while

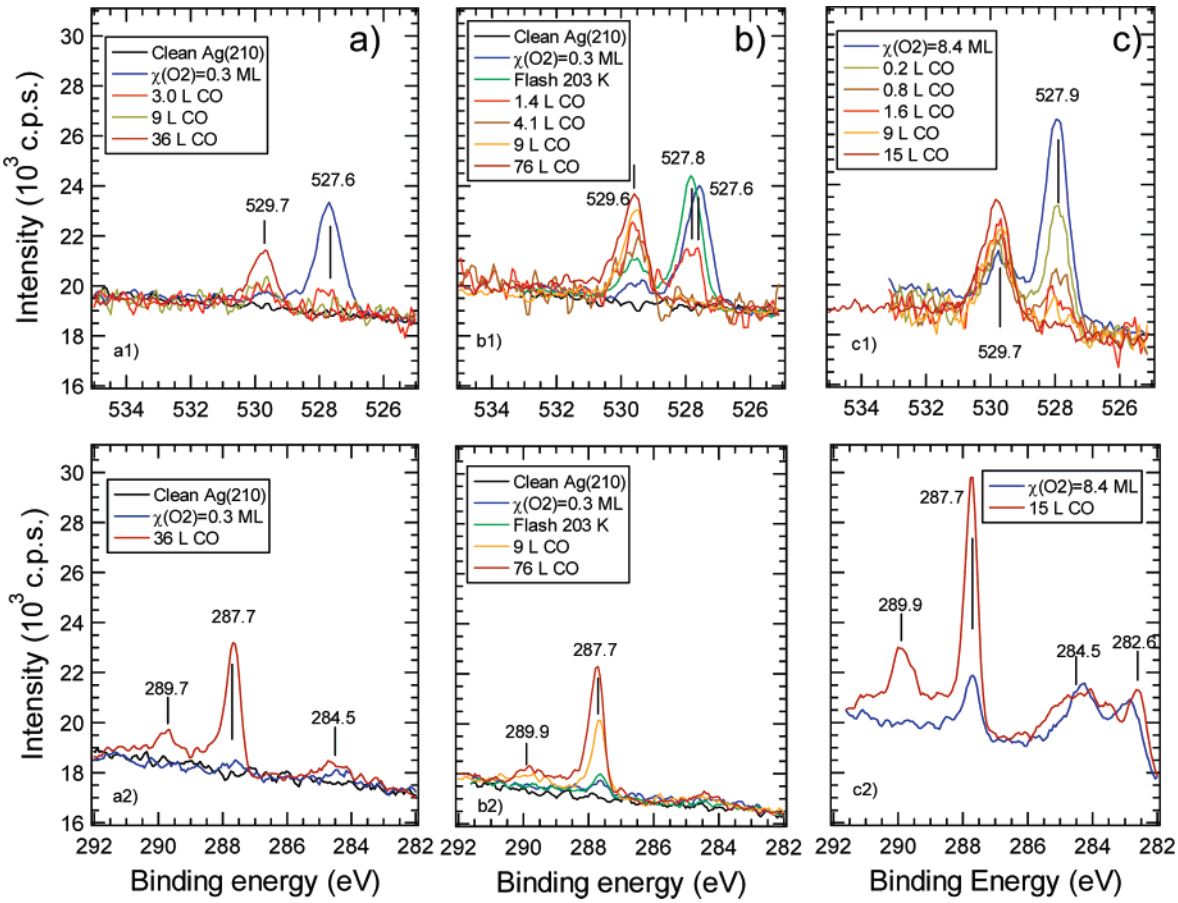

Figure 2. CO uptake on Ag(210) at 110 K exposed to different amounts of oxygen dosed by the supersonic molecular beam with $E_i = 0.40$ eV: (A) 0.3 ML O_2 dose; (B) same as in (A), but the layer was then annealed to 203 K before dosing CO to favor oxygen accumulation in the outermost subsurface layers; (C) 8.4 ML O_2 dose. For the long dose a significant amount of O_{sub} has accumulated already at 110 K. The supersurface oxygen species is rapidly removed by CO, while a significant increase of the 529.6 eV peak occurs. The presence of carbonates was checked by inspection of the C1s region before and after the CO dose (peak at 287.7 eV). Quantitative analysis shows that the 529.6 eV feature is due both to carbonate formation and to CO_3-induced subsurface accumulation. The 0.2 eV shift toward higher binding energy of the O1s peak upon annealing is connected to the disappearance of the 31 meV mode in the HREELS spectra.[14]

the other modes move to 38 and 51.5 meV, respectively. Their assignment is more complicated and can be addressed only by comparison with XPS and theoretical results (discussed later).

Figure 1B shows the corresponding XPS experiment. Two peaks are present in the O1s region upon dosing O_2 at 110 K. The one at binding energy $E_B = 527.7$ eV is assigned to oxygen adatoms ($\Theta_{O_{ad}} \approx 0.23$ ML), while the one at $E_B = 529.5$ eV includes both subsurface oxygen (O_{sub}) and carbonate contributions.[14] The latter can be estimated from the corresponding C1s signal at 287.5 eV and is initially negligible.[28] An 0.8 langmuir dose of CO at 110 K is sufficient to deplete most of the 527.7 eV intensity, suggesting that the O adatom layer is highly reactive. The slight growth of the signal at 529.5 eV and the corresponding increase in the C1s intensity at 287.5 eV indicate the formation of a small amount of carbonate,[29] while most of the oxygen is removed in the form of $CO_2\uparrow$. The CO oxidation probability, P_r, estimated from these data for $T = 110$ K is ~0.6 for small CO exposures. This value is larger than for CO−O/Ag(110) ($P_r \approx 0.03$[30]) and much larger than for CO−O/Ag(100) ($P_r < 10^{-5}$ [31]), for which little or no O removal occurs under clean conditions. The reaction rate decreases with temperature as expected for a Langmuir−Hinshelwood mechanism.

To better focus on the carbonate chemistry at the surface, we report in Figure 2 further CO uptakes on O/Ag(210) at 110 K. Experiments a and b correspond to the same, very short oxygen dose, leading to an adatom coverage $\Theta_{O_{ad}}$ of 0.12 ML and to a subsurface concentration $\Theta_{O_{sub}} < 0.002$ ML. In experiment b the surface was annealed to 203 K before dosing CO to favor oxygen accumulation from deeper layers into the outermost subsurface layer.[14] $\Theta_{O_{sub}}$ was then 0.040 ML. Experiment c corresponds to a longer O_2 dose ($\Theta_{O_{ad}} = 0.24$ ML), in which a significant amount of O_{sub} has accumulated already at 110 K ($\Theta_{O_{sub}} = 0.025$ ML). The estimated coverage for the different oxygen species and for CO_3 is reported in Table 1. We notice the following: (1) As in the case of Figure 1, O adatoms are highly reactive toward CO for all starting conditions. (2) After a few langmuirs of CO exposure, significant carbonate formation has occurred, which continues also when the O adatom layer is depleted. This is indicative that carbonates can form also by reactions involving O_{sub}, although with small efficiency. (3) The final amount of carbonates, as estimated from the C1s area at 287.7 eV, is nearly the same in experiments a and b and it is larger in experiment c, due to the larger availability of O adatoms.[32]

In all cases both O_{sub} and carbonates contribute to the intensity around 529.5 eV. From the deconvolution of this peak we can estimate the relative population of the two species after CO exposure (see Table 1). At the end of experiment a, there are about two O_{sub} atoms for each CO_3 molecule; such a ratio increases to ~6 and ~3.3 for experiments b and c, respectively. Since in these last cases some CO_3 had already formed during

TABLE 1: Estimated Coverages (ML) of Super- and Subsurface Oxygen and of CO_3 before and after CO Exposure for the Experiments of Figure 2[a]

		experiment a	experiment b	experiment c
before CO exposure	$\Theta_{O_{ad}}$	0.12	0.12	0.24
	$\Theta_{O_{sub}}$	<0.002	0.040	0.025
	Θ_{CO_3}	<0.002	<0.005	~0.008
χ_{CO} (langmuirs)		36	76	15
after CO exposure	$\Theta_{O_{ad}}$	<0.005	<0.005	0.02
	$\Theta_{O_{sub}}$	0.030	0.090	0.100
	Θ_{CO_3}	0.015	0.015	0.030
	O_{sub}/CO_3	2.0	6.0	3.3
	$\Delta O_{sub}/\Delta CO_3$		~3.9	~3.4

[a] The last two rows report the ratio between the O_{sub} and CO_3 concentrations and between the increments in the O_{sub} and CO_3 concentrations before and after CO exposure. The coverage of oxygen adatoms is determined from the 527.9 eV peak area; it is calibrated on O_2 uptake measured with the retarded reflector method and performed under conditions for which no or very little subsurface migration occurs. The O_{sub} and CO_3 coverages are estimated from the 529.7 eV peak area after deconvolution of the two contributions.[14] We assumed that the detection efficiency for these species is the same as for O adatoms. Since it is reasonable that O in a subsurface location is partially screened, this approximation leads possibly to an underestimation of the amount of O_{sub}, which however does not affect the validity of our interpretation of the data. This analysis could not be performed for intermediate CO exposures since it was not possible to record O1s and C1s spectra simultaneously during time-resolved experiments. The coverage of the other C species is not reported in the table. We estimate it to be less than 0.04 ML in experiment c, i.e., in the worst case, assuming the same C detection efficiency as for CO_3.

the preparation of the O layer, also the increment ratio $\Delta O_{sub}/\Delta CO_3$ is significant. This quantity is calculated after subtracttion of the initial O_{sub} and CO_3 contributions from the corresponding final values, so that the effect of CO exposure is evidenced and reads ~3.9 and ~3.4, respectively. The largest O_{sub}/CO_3 ratio is reached in experiment b, for which the availability of subsurface O is enhanced by annealing. Approximately six O_{sub} atoms are then present for each carbonate, and the final amount of O_{sub} is indeed close to that reached in experiment c. Quantitative analysis of the CO_3 and O_{sub} contributions clearly indicates that subsurface O has accumulated during carbonate formation and that the efficiency of this process depends on the initial availability of O both above and below the surface and/or in deeper subsurface layers (not contributing to the XPS signal). We propose the following qualitative picture: during the O_2 dose oxygen partly adsorbs on the surface and partly diffuses to the deep and near subsurface region,[15] so that the latter can act as a reservoir of oxygen atoms at a later time. During CO oxidation, oxygen adatoms are totally removed in the form of $CO_2\uparrow$ so that, when the process is completed, only CO_3 groups (E_B(O1s) = 529.6 eV[14]) are present on the surface (as witnessed by the disappearance of the 527.9 eV peak). In this stage there is no diffusion of adatoms into a subsurface location.[33] The increase of the O_{sub} concentration is due, on the contrary, to the stabilization in the subsurface layer of oxygen atoms emerging from the deep subsurface region. The presence of a CO_3 group on the surface causes a deepening of the potential well for the oxygen atom underneath; thus, the probability that the oxygen atom diffuses into that site is larger than the probability that it diffuses out of it and back into the deep region.

The final CO_3 coverage attained in the present experiments is always quite low, reading ~0.03 ML for experiment c. Moreover, the amount of oxygen accumulated in subsurface sites is up to 4 times larger in the presence of carbonates than in the presence of O adatoms, in spite of the much smaller coverage of the former species. Thus, the overall picture strongly suggests that carbonates are far more efficient than O_{ad} in stabilizing subsurface oxygen. Due to their low coverage a lot of free adsorption sites are left available for adsorption of further reactants, which may possibly interact with O_{sub}.

The reservoir of dissolved O is unavoidably refilled in each experiment during the initial oxygen exposure, even at the lowest investigated temperature. In accord with this no subsurface oxygen accumulation nor carbonate formation occurs in blank experiments in which CO is dosed on a surface not previously exposed to O_2.

Finally, we mention that the spectra in Figure 2C, i.e., those corresponding to the largest O_2 exposure, show two broad features at E_B = 282.6 and 284.5 eV, which have no correspondence in the O1s region. The former value is compatible with carbidic carbon. The intensity of this line increases at the expense of that at 284.5 eV when the crystal is annealed to 200 K and persists up to 300 K (not shown). We assign both signals to atomic C at the surface and in the immediate subsurface region, respectively. These peaks are significant only upon large O_2 exposures, indicating that C segregation is induced by O_2. Such peaks are not affected by CO exposure. This contamination does not play an active role in the O_{sub} stabilization process since (i) the C intensity does not change in Figure 2C, while the amount of O_{sub} increases upon CO exposure, i.e., with CO_3 coverage, and (ii) the amount of O_{sub} stabilized in experiment c is perfectly coherent with that found in experiments a and b, where little or no C species are present. In particular the incremental ratio $\Delta O_{sub}/\Delta CO_3$ (i.e., how many O atoms are stabilized for each additional CO_3 molecule) is compatible for experiments b and c. The only effect of the C species we can suppose is some poisoning of adsorption sites, but we do not have enough experimental evidence to prove or confute this hypothesis.

After the reaction another peak appears at 290 eV, which remains stable up to 150 K. Again no correlated O signal could be identified. Since this binding energy is typical for carbon oxides, we tentatively assign this species to a bent CO_2 moiety with the corresponding O1s line hidden in the 530 eV intensity.

Comparison of HREELS and XPS data indicates that the 38 meV loss must correspond either to the excitation of the carbonate surface vibration (the energy of this mode is 34.4 meV for Ag(110)[27]) or to a subsurface oxygen related mode. The 51.5 meV mode must, on the other hand, be connected to subsurface oxygen since no modes are present in this region for CO_3−Ag(110).

To clarify and support these findings, an extensive DFT study of Ag(210) in the presence of coadsorbed oxygen and CO_3 has been undertaken. The energetics of oxygen chemisorption in various configurations combining adsorption at the (110) step (A site), on the (100) nanoterrace (B site), and in the subsurface octahedral interstitial site under the step (Octa site) has been recently studied by some of us.[34,35] We extend this study further in this paper. In Table 2(column 3), we summarize the results

TABLE 2: Total Chemisorption Energies of Oxygen with Reference to Clean Ag(210) and Gas-Phase O_2 and CO_2 (in the Case Where CO_3 Is Attached to the Surface)[a]

oxygen coverage (ML)	structure	total E_{chem}/cell, eq 1	additional CO_3 (ML)	structure	total E_{chem}/cell, eq 2
		(2 × 1) Surface Cell			
0		0.00	1/2	CO_3	−1.72
1/4	A	−0.68	1/2	CO_3−A	−1.98
	B	−0.49		CO_3−OctaI	−1.89
	Octa	−0.07		CO_3−OctaII	−1.79
				CO_3−OctaIII	−1.61
1/2	A−A	−1.60	1/2	CO_3−A−OctaI	−2.33
	A−B	−1.12		CO_3−A−OctaII	−1.86
	B−B	−0.84		CO_3−A−OctaII I	−1.91
	A−Octa	−0.61		CO_3−Octa−Octa	−2.03
3/4	A−A−B	−1.20			
	A−A−Octa	−1.62			
1	A−A−Octa−Octa	−1.63			
		(2 × 2) Surface Cell			
0		0.00	1/4	CO_3	−2.01
1/8			1/4	CO_3−Octa	−2.07
2/8			1/4	CO_3−2 × Octa	−2.55
3/8			1/4	CO_3−3 × Octa	−2.83

[a] CO_3−2 × Octa is two Octa oxygens in the presence of CO_3, and CO_3−3 × Octa is 3 Octa oxygens in the presence of CO_3.

of the total oxygen chemisorption energies calculated in the (2 × 1) surface unit cell, with respect to the clean Ag(210) surface and to molecular oxygen in the gas phase, using the equation

$$E_{chem}(O) = [E_{O/Ag} - E_{Ag} - N_O(E_{O_2}/2)] \quad (1)$$

where $E_{O/Ag}$ is the energy of the slab with oxygen adsorbed on/in it, E_{Ag} is the energy of the clean Ag slab, E_{O_2} is the energy of O_2 in the gas phase, and N_O is the number of oxygen atoms adsorbed on the surface. From these results we can see that subsurface oxygen by itself (adsorption energy −0.07 eV) is not thermodynamically stable with respect to adsorption at the step (−0.68 eV) or at the terrace (−0.49 eV). It is however stable with respect to an oxygen in an Octa site in the bulk (0.67 eV, as calculated in a 64 Ag atom fcc supercell). With increasing oxygen dosing, initially step sites are occupied, and when all steps are fully decorated by −O−Ag−O−Ag− chains, further oxygen prefers to move subsurface (A−A−Octa, −1.62 eV) rather than occupy terrace sites (A−A−B, −1.20 eV). However, the thermodynamic driving force for subsurface oxygen accumulation is extremely weak, and there is no significant gain in energy when further oxygen is adsorbed subsurface (A−A−Octa−Octa, −1.63 eV). From the results reported in the table it can be concluded that, in the absence of carbonates, oxygen adsorbs preferentially at step sites and migrates subsurface only when the steps are fully decorated. We find that the step oxygen is negatively charged by about −1 charge unit and step Ag atoms are positively charged. The attraction between negative subsurface oxygen and the positive step Ag atoms could explain in part the increase in subsurface oxygen adsorption with an increase in step oxygen coverage.

As for CO_3/Ag(210), we considered CO_3 formed by one oxygen at the step site and one CO_2 molecule attached to it. We tried various orientations of CO_3 with respect to the (110) step, and the most favorable configurations were those where one oxygen is at the step edge and the other two oxygens are adsorbed on the lower terrace. All other configurations where the two nonstep oxygens are not bonded to any Ag atom are higher in energy. In Figure 3 we show one typical configuration of this kind where the adsorbed CO_3 molecules display a symmetry-breaking clockwise rotation around the surface normal.[36] Since the main effect of CO dosing in the experiment is the removal of oxygen from the surface in the form of gas-phase CO_2, we report in Table 2 the total chemisorption energies, always for a (2 × 1) surface cell, computed by taking gas-phase O_2 and CO_2 as references and using the equation

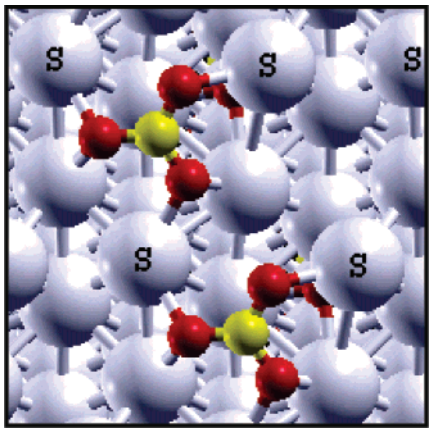

Figure 3. A typical starting configuration of the Ag(210) surface with CO_3 adsorbed parallel to the (110) step along with a subsurface oxygen below the step atoms. Atoms marked "S" are the step Ag atoms.

$$E_{chem}(O_2,CO_2) = [E_{CO_3+O/Ag} - E_{Ag} - N_O E_{O_2}/2 - E_{CO_2}] \quad (2)$$

In Figure 4a, we show a schematic projected top view of the Ag(210) surface in which open circles are the Ag atoms and the thick line marks the (2 × 1) unit cell. There are two possible Octa sites in a cell right below the step atoms. When CO_3 is not adsorbed, both Octa sites are the same. However, when we adsorb CO_3 along with one oxygen at an Octa site, we get different local minima corresponding to rotation of the CO_3 molecule with respect to the subsurface oxygen. In Figure 4b, we show the CO_3−OctaI structure, where the step oxygen of CO_3 has moved toward the subsurface oxygen. We then took the structure of Figure 4b and rotated CO_3 anticlockwise. After relaxing this new configuration, we got the structure shown in Figure 4c, where one of the legged oxygens of CO_3 has come toward the subsurface oxygen. We call this structure CO_3−OctaII. We again took the structure from Figure 4b and moved the subsurface oxygen from its current position to the other Octa site in the cell, keeping the clockwise rotation of CO_3. After

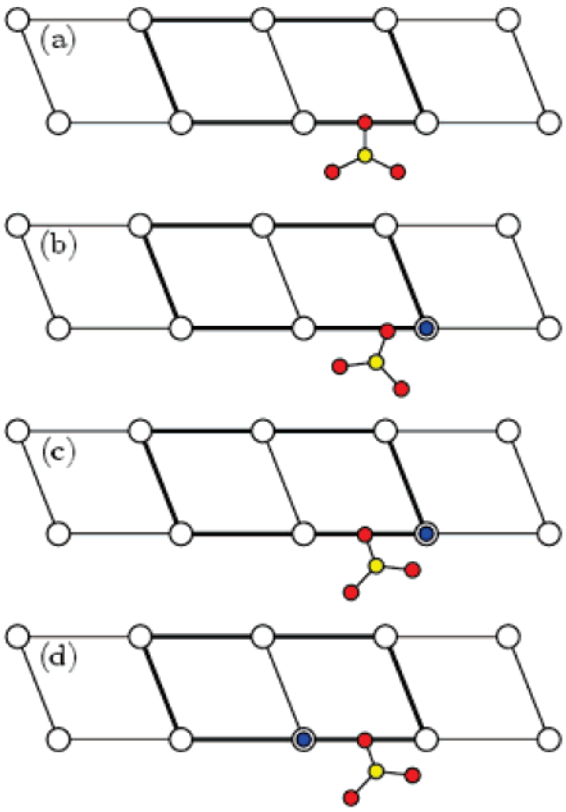

Figure 4. (a) is a projected top view of the Ag(210) surface, (b), (c), and (d) are the CO_3−OctaI, CO_3−OctaII, and CO_3−OctaIII structures, respectively. Open circles are the step Ag atoms, red circles are oxygen atoms of CO_3, the yellow circle is the carbon atom, and the blue atom right below the step Ag atom is subsurface (Octa) oxygen. The cell shown by thick lines is the (2 × 1) unit cell.

relaxing this initial configuration, we found that the step oxygen had not moved toward the subsurface oxygen (Figure 4d) as much as it had in Figure 4b, and we call this structure CO_3−OctaIII. From Table 2 it can be appreciated that, at variance with the pure oxygen adsorption case where subsurface occupation (Octa, −0.07 eV) is clearly less favorable than step adsorption (A, −0.68 eV), in the presence of CO_3 the adsorption energy of some configurations including subsurface oxygen (CO_3−OctaI, −1.89 eV; CO_3−OctaII, −1.79 eV) becomes comparable to that for step adsorption (CO_3−A, −1.98 eV).

The tendency of carbonate to stabilize subsurface oxygen is confirmed considering configurations with more subsurface oxygen. A structure with oxygen atoms adsorbed in the octahedral sites under both the nonstep oxygen atoms of the CO_3 molecule has lower chemisorption energy (is more stable) than those corresponding to a single subsurface oxygen per CO_3 molecule. The tendency of the subsurface oxygen to migrate to step sites is also very much reduced in this case: compare the 0.30 eV adsorption energy difference between the CO_3−Octa−Octa and the CO_3−A−OctaI configurations with the 0.99 eV difference between the A−Octa and A−A structures or the 0.61 eV difference between the A and Octa structures in Table 2.

The results obtained in the (2 × 1) surface unit cell correspond to an extremely large carbonate coverage as compared with the experimental situation. We therefore performed additional calculations for the larger (2 × 2) surface supercell, corresponding to a CO_3 coverage of 0.25 ML. These results are also reported in Table 2. We found that the chemisorption energy of CO_3 increases as we decrease the coverage, and this happens because CO_3 gets negatively charged (about −1) on the surface,

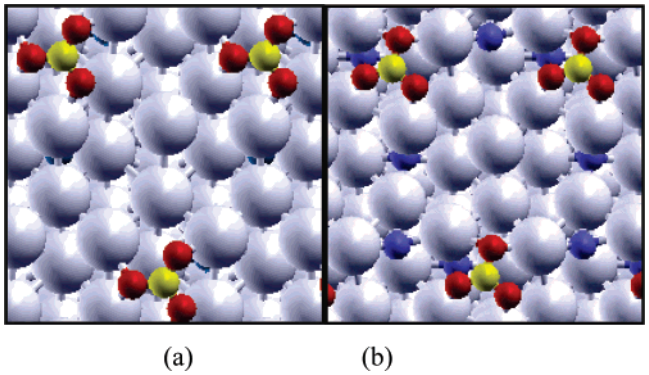

Figure 5. Initial (unrelaxed (a)) and final (relaxed (b)) structures for a (2 × 2) cell with a 0.25 ML CO_3 coverage and three subsurface oxygens.

leading to a repulsive interaction among CO_3 molecules. Again we found that the total chemisorption energy of subsurface oxygen increases with the number of subsurface oxygens, and for instance, we found that E_{chem} with three subsurface oxygen atoms is 0.28 eV lower than E_{chem} with two subsurface oxygen atoms. In this case the surface geometry is heavily distorted, as shown in Figure 5. In the starting configuration (unrelaxed structure a), the subsurface oxygens are covered by Ag surface atoms; however, due to the presence of CO_3, the crystal structure strongly relaxes (structure b), exposing the subsurface oxygen atoms (blue spheres) and thus justifying the experimental detection of their vibrations by HREELS. The stability of subsurface oxygen is thus due in part to the CO_3-induced distortion of the crystal that makes the subsurface sites more easily accessible and in part to the attraction between the subsurface oxygen and the positively charged Ag atoms bonded to CO_3. The high CO_3 coverage considered here puts constraints on the allowed crystal distortion pattern. We expect that moving to even lower coverage (closer to the experimental values) will further stabilize subsurface oxygen. Indeed, moving from 0.5 to 0.25 ML coverage, the stability of subsurface oxygen increases by 0.18 eV for CO_3−OctaI and by 0.52 eV for CO_3−Octa−Octa.

To further support the oxygen tendency to accumulate subsurface in the presence of carbonate, we studied the vibrational signatures of three representative $CO_3 + O_{sub}$/Ag structures in the (2 × 1) surface geometry: CO_3−OctaI, CO_3−OctaII, and CO_3−Octa−Octa. In all three cases the highest calculated vibrational frequency is at 95 meV, corresponding to the vibration of carbon against the plane of carbonate oxygen atoms (Figure 6). The corresponding measured value is 101 meV, and the discrepancy is due to the PBE functional used in our calculation. The frequency of the same mode calculated in gas-phase H_2CO_3 is 94 meV, from both the present and the previous DFT−GGA calculation,[37] while the well-established experimental value for the same mode is 100 meV.[38] The most interesting modes for the present purpose are those involving a strong motion of subsuface oxygen. In both structures with one subsurface oxygen per carbonate, CO_3−OctaI and CO_3−OctaII, these modes have frequencies in the 38−46 meV range, somewhat low compared with the 51.5 meV of the measured frequency. Supersurface oxygen (oxygen in the CO_3 molecules) vibrates for these surfaces in the range 30−35 meV.

The phonon calculations on the CO_3−Octa−Octa structure reveal instead an interesting mode corresponding to a concerted motion of the two subsurface oxygen atoms at 50 meV, which compares well with the experimentally observed mode at 51.5 meV. These results suggest that, to display a vibrational

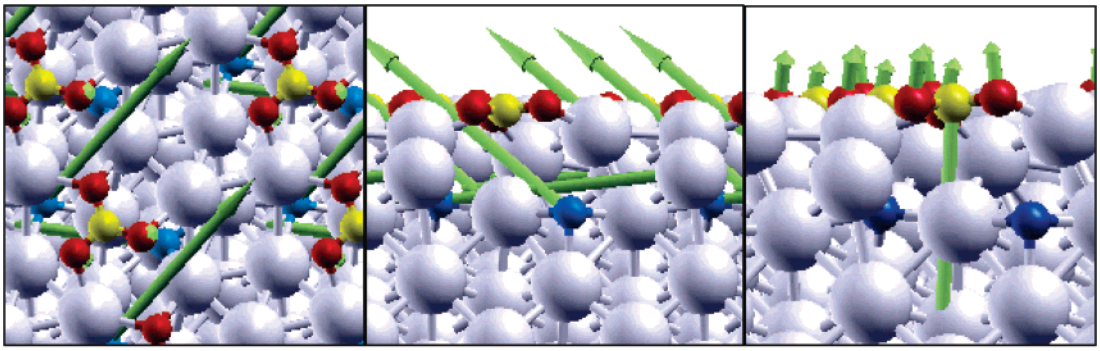

Figure 6. (a) Top view of the eigenvector corresponding to the 38 meV mode. Primarily, the two subsurface oxygens vibrate at an angle of almost 60° with respect to the surface normal with a very small amplitude of the carbonate−oxygen motion. Blue spheres represent the subsurface oxygens. (b) Side view of the mode corresponding to the 50 meV frequency. Only subsurface oxygens vibrate at an angle of almost 120°. (c) Side view of the out-of-plane bending mode of CO_3, observed at 95 meV, where carbon vibrates out of phase with the three oxygens.

TABLE 3: Vibrational Frequencies (meV) of O_{sub}, $CO_3 + O_{sub}$, and CO_3 in the Three Structures CO_3−OctaI, CO_3−OctaII, and CO_3−Octa−Octa As Obtained in DFPT Calculations[a]

species	CO_3−OctaI	CO_3−OctaII	CO_3−Octa−Octa
Ag modes	0−20	0−20	0−20
O_{sub}	38,[b] 43[b]	37,[b] 41,[b] 46[c]	38,[d] 40,[d] 41,[d] 44,[e] 50[e]
$CO_3 + O_{sub}$	34	34	31, 32, 35
CO_3	30, 81, 82, **95**, 126, 151, 170	30, 80, 82, **95**, 125, 158, 170	81, 82, **95**, 126, 168

[a] The bold-faced frequency of 95 meV (out-of-plane bending mode of CO_3) observed for all three structures is the vibration with the highest vertical component. Most other modes of CO_3 vibration are planar, and small vertical components are present only for a few cases. [b] Strong vertical component. [c] Mostly in-plane vibration. [d] Very small CO_3 vibration. [e] One oxygen vibrates vertically and the other in-plane.

peak at the observed frequency, more than one subsurface oxygen atom per carbonate molecule is needed, thus indirectly supporting the conclusion that more than one subsurface oxygen is stabilized by each CO_3 in the present experimental conditions. For the same structure, there are other modes in the range of 38−45 meV which also involve subsurface oxygen motion and modes in the range of 30−35 meV involving supersurface oxygen motion. This suggests that the experimentally observed loss at 38 meV is due to the combined sub- and supersurface oxygen vibration. In addition, we get the usual CO_3 out-of-plane bending mode at 95 meV. All results compare very well with the experimentally measured energies of 38, 51.5, and 101 meV; in Figure 6, we show the calculated vibrational eigenmodes corresponding to these frequencies. In Table 3, we give the values of the frequencies for O_{sub}, $CO_3 + O_{sub}$, and CO_3 vibrations for all three structures CO_3−OctaI, CO_3−OctaII, and CO_3−Octa−Octa.

According to our calculations, the vibrational modes detected by HREELS mainly involve subsurface oxygen motion. Their detection is possible due to the heavy distortion of the CO_3-covered surface (Figure 5), which reduces the screening of subsurface oxygen. These findings confirm the mode assignment and further support the conclusion that CO_3 stabilizes accumulation of O_{sub} as found in the experiments.

We notice finally that the present results are in accord with our previous XPS data on CO oxidation at Ag(100),[39,40] which showed the growth of a photoemission feature close to the Fermi level when CO was dosed above room temperature. This feature was assigned by DFT calculations to the formation of a surface oxide phase and implied O accumulation in subsurface sites induced by the transient adsorption of the CO molecules after supersurface oxygen was removed. The geometry of that surface did not allow, however, identification of a well-defined signal to be associated with O in subsurface sites as can be done for Ag(210).

Conclusions

In conclusion, we have shown that CO_3 formed on the Ag(210) surface during CO oxidation induces oxygen accumulation in the subsurface region and stabilizes this species more efficiently than O adatoms. Such O_{sub} will eventually be available for further reactions, especially considering that the large majority of supersurface sites are still free for adsorption of other reactants from the gas phase. This finding might help in clarifying some effects so far unexplained, e.g., the activation of polycrystalline Ag films for ethylene epoxidation by pretreatment with CO and O_2 mixtures in the 10^{-2} mbar range[7,8] and the high activity of Ag powders under catalytic conditions, in which carbonates are surely present on the surface.

Acknowledgment. We acknowledge financial support by MIUR under PRIN 2003, G. Rovida for providing the Ag(210) sample, and the SuperESCA staff for technical support.

References and Notes

(1) Somorjai, G. A. *Introduction to Surface Chemistry and Catalysis*; Wiley: New York, 1994.
(2) Van den Hoek, P. J.; Baerends, E. J.; Van Santen, R. A. *J. Phys. Chem.* **1989**, *93*, 6469.
(3) Van Santen, R. A.; Kuipers, H. P. C. *Adv. Catal.* **1987**, *35*, 265.
(4) Serafin, J. G.; Liu, A. C.; Seyedmonir, S. R. *J. Mol. Catal. A: Chem.* **1998**, *131*, 157.
(5) Nagy, A. J.; Mestl, G.; Schloegl, R. *J. Catal.* **1999**, *188*, 58.
(6) Qu, Z.; Cheng, M.; Huang, W.; Bao, X. *J. Catal.* **2005**, *229*, 446.
(7) Grant, R. B.; Lambert, R. M. *J. Catal.* **1985**, *92*, 364.
(8) Bukhtiyarov, V. I.; Kondratenko, V. A.; Boronin, A. I. *Surf. Sci.* **1993**, *293*, L826. Bukhtiyarov, V. I.; Boronin, A. I.; Prosvirin, I. P.; Savchenko, V. I. *J. Catal.* **1994**, *150*, 268.
(9) Bukthiyarov, V. I.; Nizovskii, A. I.; Bluhm, H.; Haevecker, M.; Kleimenov, E.; Knop-Gericke, A.; Schloegl, R. *J. Catal.* **2006**, *238*, 260.
(10) Atkins, M.; Couves, J.; Hague, M.; Sakakini, B. H.; Waugh, K. C. *J. Catal.* **2005**, *235*, 103.
(11) Stegelmann, C.; Stoltze, P. *J. Catal.* **2004**, *226*, 129.
(12) Bertole, C. J.; Mims, C. A. *J. Catal.* **1999**, *184*, 224.

(13) Nagy, A.; Mestl, G.; Herein, D.; Weinberg, G.; Kitzelmann, E.; Schloegl, R. *J. Catal.* **1999**, *182*, 417. Rehren, C.; Muhler, M.; Bao, X.; Schloegl, R.; Ertl, G. *Z. Phys. Chem. (Muenchen)* **1991**, *174*, 11. Bao, X.; Muhler, M.; Pettinger, B.; Schloegl, R.; Ertl, G. *Catal. Lett.* **1993**, *22*, 215. Grant, R. B.; Lambert, R. M. *J. Catal.* **1985**, *92*, 364.

(14) Savio, L.; Gerbi, A.; Vattuone, L.; Baraldi, A.; Comelli, G.; Rocca, M. *J. Phys. Chem. B* **2006**, *110*, 942.

(15) Vattuone, L.; Savio, L.; Rocca, M. *Phys. Rev. Lett.* **2003**, *90*, 228302.

(16) Bonini, N.; Dal Corso, A.; Kokalj, A.; de Gironcoli, S.; Baroni, S. *Surf. Sci.* **2005**, *587*, 50.

(17) Abrami, A.; Barnaba, M.; Battistello, L.; Bianco, A.; Brena, B.; Cautero, G.; Chen, Q. H.; Cocco, D.; Comelli, G.; Contrino, S.; DeBona, F.; Di Fonzo, S.; Fava, C.; Finetti, P.; Furlan, P.; Galimberti, A.; Gambitta, A.; Giuressi, D.; Godnig, R.; Jark, W.; Lizzit, S.; Mazzolini, F.; Melpignano, P.; Olivi, L.; Paolucci, G.; Pugliese, R.; Qian, S. N.; Rosei, R.; Sandrin, G.; Savoia, A.; Sergo, R.; Sostero, G.; Tommasini, R.; Tudor, M.; Vivoda, D.; Wei, F.-Q.; Zanini, F. *Rev. Sci. Instrum.* **1995**, *66*, 1618.

(18) Rocca, M.; Valbusa, U.; Gussoni, A.; Maloberti, G.; Racca, L. *Rev. Sci. Instrum.* **1991**, *62*, 2172.

(19) Baraldi, A.; Comelli, G.; Lizzit, S.; Kiskinova, M.; Paolucci, G. *Surf. Sci. Rep.* **2003**, *49*, 169.

(20) The relative sensitivity to C and O was evaluated by comparing the areas of the photoemission peaks measured for CO_2 adsorption. Also all the coverages deduced from XPS are evaluated on the basis of the peak areas. We underline that a raw comparison of the O1s and C1s peak intensities can be misleading since the C1s level is sharper than the O1s level.

(21) Citrin, P. H.; Wertheim, G. K.; Baer, Y. *Phys. Rev. B* **1983**, *27*, 3160.

(22) Baroni, S.; Dal Corso, A.; de Gironcoli, S.; Giannozzi, P. PWscf and PHONON: Plane-wave pseudo-potential codes. http://www.quantum-espresso.org/, 2001.

(23) Vanderbilt, D. *Phys. Rev. B* **1990**, *41*, 7892.

(24) Perdew, J. P.; Burke, K.; Ernzerhof, M. *Phys. Rev. Lett.* **1996**, *77*, 3865.

(25) Methfessel, M.; Paxton, A. T. *Phys. Rev. B* **1989**, *40*, 3616.

(26) Monkhorst, H. J.; Pack, J. D. *Phys. Rev. B* **1990**, *13*, 5188.

(27) Constant, L.; Kreuzer, B.; Stenzel, W.; Conrad, H.; Bradshow, A. M. *Surf. Sci.* **1999**, *427*−*428*, 262.

(28) The relative weights of the O_{sub} and CO_3 contributions to the 529.7 eV peak are calculated from the formulas $A(O_{CO_3}) = A(287.7\ \text{eV})(3/7.5)$ and $A(O_{sub}) = A(529.7\ \text{eV}) - A(O_{CO_3})$, considering that the detection efficiency for C is 7.5 times larger than that for oxygen in our experimental conditions and that there are three O atoms for each C atom in CO_3. Conversion to MLs occurs by admitting the same detection efficiency for O_{sub}, for O_{CO_3}, and for O_{ad}, for which a direct calibration through retarded reflector method experiments was possible.

(29) Campbell, C. T.; Paffett, M. T. *Surf. Sci.* **1984**, *143*, 517.

(30) Burghaus, U.; Conrad, H. *Surf. Sci.* **1995**, *338*, L869.

(31) Burghaus, U.; Vattuone, L.; Gambardella, P.; Rocca, M. *Surf. Sci.* **1997**, *374*, 1.

(32) The C1s signal of CO_3 is shifted by 0.2 eV between the spectrum of Figure 1B and that of Figure 2. The effect may be due to the larger concentration of either CO_3 or subsurface O.

(33) As a proof of this statement we observe that (i) the time evolution of the XPS spectra shows no depletion of the supersurface O signal at 110 K, (ii) the evolution with crystal temperature shows that subsurface oxygen accumulation does not occur at the expense of supersurface oxygen (see Figure 6 of ref 14), and (iii) in Figure 2A the O_{sub} related peak continues to grow also after the complete removal of the intensity at 527.9 eV (corresponding to supersurface oxygen).

(34) Bonini, N.; Kokalj, A.; Dal Corso, A.; de Gironcoli, S.; Baroni, S. *Phys. Rev. B* **2004**, *69*, 195401.

(35) Kokalj, A.; Bonini, N.; Dal Corso, A.; de Gironcoli, S.; Baroni, S. *Surf. Sci.* **2004**, *566*−*568*, 1107.

(36) An adsorption geometry displaying a symmetrical counterclockwise rotation is of course also possible and degenerate in energy.

(37) Montanari, B.; Ballone, P.; Jones, R. *Macromolecules* **1999**, *32*, 3396.

(38) Moore, M. H.; Khanna, R. K. *Spectrochim. Acta* **1991**, *47A*, 255.

(39) Rocca, M.; Savio, L.; Vattuone, L.; Burghaus, U.; Palomba, V.; Novelli, N.; Buatier de Mongeot, F.; Valbusa, U. *Phys. Rev. B* **2001**, *63*, 081404(R).

(40) Savio, L.; Vattuone, L.; Rocca, M.; Buatier de Mongeot, F.; Comelli, G.; Baraldi, A.; Lizzit, S.; Paolucci, G. *Surf. Sci.* **2002**, *506*, 213.